Advance Power Quality Awareness With High-Resolution Continuous Waveform Streaming and Recording

Richard Kirby, Ganga Ramesh, Phil Stoaks, and Drew Cannon
Schweitzer Engineering Laboratories, Inc.

This paper was presented at the 72nd Annual Petroleum and Chemical Industry Technical Conference, Dallas, TX, September 22–24, 2025.

For the complete history of this paper, refer to the next page.

Revised edition released October 2025

Originally presented at the
72nd Annual IEEE IAS Petroleum and Chemical Industry
Technical Conference (PCIC, September 2025

ADVANCE POWER QUALITY AWARENESS WITH HIGH-RESOLUTION CONTINUOUS WAVEFORM STREAMING AND RECORDING

Richard Kirby, PE
Senior Member, IEEE
Schweitzer Engineering Laboratories, Inc.
10111 Richmond Ave
Houston, TX 77042 USA
richard_kirby@selinc.com

Ganga Ramesh
Schweitzer Engineering Laboratories, Inc.
10111 Richmond Ave
Houston, TX 77042 USA
ganga_ramesh@selinc.com

Phil Stoaks
Schweitzer Engineering Laboratories, Inc.
12754 W LaSalle St
Boise, ID 83713 USA
phil_stoaks@selinc.com

Drew Cannon
Schweitzer Engineering Laboratories, Inc.
1500 NW Bethany Blvd
Beaverton, OR 97006 USA
drew_cannon@selinc.com

Abstract – Industrial power system health and power quality have become less predictable as inverter-based generation, variable speed drives (direct current drives and alternating current variable-frequency drives), and nonlinear loads are more frequently applied in industrial plants. Monitoring devices, including microprocessor-based protective relays and power quality meters, capture multiple cycles or even seconds of waveform disturbance data based on predefined event trigger conditions. These devices can fail to record the full extent of longer duration conditions, such as increased voltage distortion, voltage sags, and oscillations that can last minutes, hours, or even days. Additionally, the limited recording capabilities of traditional power quality monitoring devices commonly fail to capture disturbances, such as rapid voltage changes, switching transients, and rapid power overloads or underloads.

In this paper, these failures and challenges are addressed by continuously recording 14.4 kilosamples per second voltage and current waveform information. The recorded data provide troubleshooting information and allow analysis of any disturbance that occurs on the power system. Several real-world events demonstrate the value of continuous waveform recording, and the paper explains the benefits of newer waveform data.

Index Terms — Power quality, nonsinusoidal, time-synchronized, continuous waveform measurement, oscillography, streaming, recording, subcycle disturbance

I. INTRODUCTION

The understanding and awareness of the condition and quality of industrial power systems are only as complete as the tools used to monitor system behavior and performance. Visualization and equipment failure identification require measurements obtained by triggering and capturing waveform data [1]. Conventional power quality monitors capture disturbance data based on predefined trigger conditions that can be anywhere from multiple cycles to multiple seconds long. However, certain system disturbances, such as voltage sags and interruptions, can last for minutes, exceeding the preset recording window in these devices. Users must have thorough knowledge of power quality disturbances to correctly configure trigger conditions, such as harmonic or voltage pickup thresholds, with disturbance records of limited duration. Too sensitive, and the monitoring device will trigger too often and overwrite valuable data. Not sensitive enough, and the equipment will fail to record actual power disturbances. Continuous waveform streaming and recording (CWS&R) entirely resolves the trigger condition issues by producing gapless and triggerless waveform measurement signals. The recording window is limited primarily by the system's storage capacity.

Industrial power systems have become more and more unbalanced and distorted with the growing number of nonlinear loads, like induction furnaces and variable speed drives, and with the increasing penetration of inverter-based generation [1] [2] [3]. Conventional power quality monitors calculate time-averaged power, voltage, current, and other measurements over a half cycle or more. A typical averaging time for power quality measurements is 10 or 12 cycles (200 ms) [4]. This measurement period provides acceptable accuracy and dampens signal changes, but averages out one-cycle or subcycle disturbances. Power monitoring equipment may fail to capture disturbances like rapid voltage changes, power oscillations, and switching transients. By contrast, modern power monitors and digital disturbance recorders can continuously stream and record discrete time-sampled data at millisecond or microsecond rates to provide accurate disturbance data with more resolution.

This paper presents data from CWS&R systems that provide high-bandwidth, discrete time-sampled current and voltage signals. Figure 1 shows the components of a CWS&R system, including a waveform measurement unit (WMU), continuous waveform recording (CWR) software, and a Global Positioning System (GPS) clock.

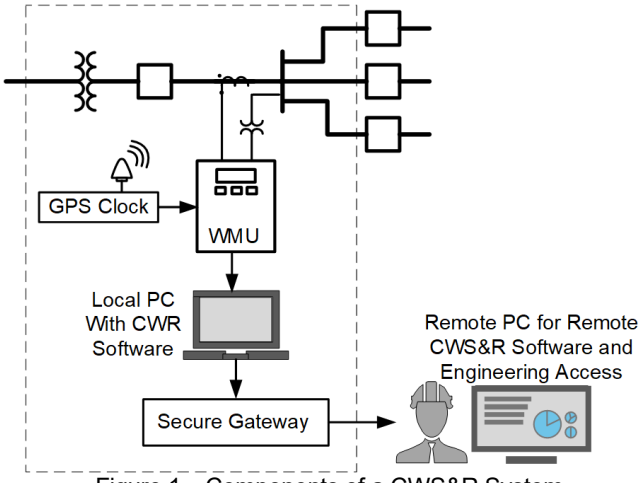

Figure 1 Components of a CWS&R System

This CWS&R system consists of a WMU, which is a power monitor that produces and streams continuous waveform signals at a constant sampling rate. 14.4 kilosamples per second (ksps) is an industry-preferred reporting rate for power quality metering applications, per Table 902 – Standard sample rates in [5], due to being exactly divisible by 50 and 60. This rate equals 288 samples per cycle (spc) at 50 Hz and 240 spc at 60 Hz. The continuous waveform streaming (CWS) signals are time-synchronized to an accurate time source. The streamed data are recorded using CWR software on a local computer. This CWR software provides a web browser-based visualization of the waveform measurements that a user can access for monitoring and analysis from a local or remote computer.

The CWS&R system stores the time-synchronized data at a fixed rate and can precisely correlate with other local or wide-area networks. Communication network delays do not affect data correlation given each data sample includes a high-precision time stamp allowing data comparison from WMUs at various locations across the system [6] [7].

The WMU 14.4 ksps voltages and currents streaming rate, without onboard triggered waveform recording, limits the applications to a signal bandwidth of 6 ksps or 6 kHz (100th harmonic at 60 Hz or 120th harmonic at 50 Hz). The higher the streaming rate the finer the time resolution and greater the signal bandwidth. Detection and recording of microsecond step change transients, electromagnetic traveling waves (TWs), and distortion measurements up to 150 kHz require 1 megasample per second (Msps) (samples time-stamped with a resolution of 1 µs) with 400 kHz of signal bandwidth, or higher, waveform recording, and related instrument transformers [8].

This paper discusses the benefits of using WMU signals for capturing and analyzing transients, subcycle disturbances, and voltage and current distortion. Section II of this paper discusses how WMU signals compare against the data from a supervisory control and data acquisition (SCADA) system and time-synchronized signals from phasor measurement units (PMU). Section III describes how the CWR software can be used to derive synchrophasor data from waveform measurements. Section IV highlights the use of waveform recordings and analyses at an iron casting plant. Section V discusses network bandwidth and data considerations.

II. SCADA, PMU, AND WMU SIGNALS

SCADA systems are common in modern power systems. These systems monitor time-averaged voltage, current, and power magnitudes that are useful for long-term energy management. SCADA measurements typically update every 1 to 6 s, as shown in Figure 2. SCADA measurements obtained from various locations in the monitored system are generally not synchronized to a common time reference. Lack of time-synchronization and a relatively low update rate limit the ability of a SCADA system to monitor some types of system disturbances or improve situational awareness.

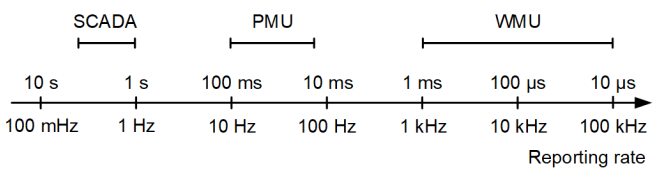

Figure 2 Reporting Rates of SCADA, PMUs, and WMUs [9]

In recent decades, PMUs have helped improve the visibility of real-time system dynamics, such as power and frequency oscillations. That said, since PMUs report measurements only at frequencies near the fundamental frequency, they cannot aid in the detection and observation of subcycle and higher-frequency disturbances. (See Section III-B for a discussion of PMU signal spectral content.) Unlike SCADA systems, PMU measurements are time-synchronized to a common precise time reference, such as a GPS clock, and are therefore called synchrophasors [10]. PMU measurements are typically updated at 25 or 50 samples per second (sps) for 50 Hz systems and at 30 or 60 sps for 60 Hz systems, which is a much higher sampling rate than SCADA measurements.

While PMUs provide time-synchronized phasor measurements, WMUs provide time-synchronized, instantaneous waveform-sampled signal measurements of voltages and currents. These raw signal data offer a more accurate representation of the voltage and current and, as a result, can assist in detecting rapid power oscillations or high-frequency transients. The data can also assist in monitoring the dynamic response of the system to these disturbances. WMUs and PMUs share several useful characteristics. For example, they both require a precise 10 µs, or better, time source, making WMUs an extension of traditional PMUs. WMUs have significantly higher reporting rates, such as 14.4 ksps, and therefore have a higher-signal bandwidth when compared to PMUs. This distinction makes WMUs the better representation of signal measurements, particularly during transient events [7]. Additionally, since PMU signals calculate the magnitude and angle only at the fundamental frequency and not at multiples of the fundamental, as proposed with harmonic PMUs, derived quantities, such as total harmonic distortion (THD), cannot be calculated. With WMU data, THD can be calculated in software from the waveform measurements at each WMU location within the power system [7]. Furthermore, the harmonic PMU signals can also be derived from the WMU signals and applied as described in [8].

TWs are launched by high-frequency power system events, including transmission faults, lightning strikes, circuit breaker reignition or restrike, breaker transient recovery voltages faults, partial discharge, switching, and fault precursors (incipient faults). An ultra-high-speed transmission relay with TW fault-locating capability captures and records triggered 1 Msps and 10 ksps waveform records within the device [11] [12]. Triggered 1 Msps records that use voltage-based or current-based TW disturbance detectors may still fail to capture a record due to 1) faults that launch small TWs (point-on-wave challenge), 2) low-amplitude nonfault inception TWs, and 3) faults that are very close to a transmission line terminal (TWs that frequently reflect and overlap) [12]. IEC recommends a 96 ksps WMU for high-bandwidth direct current (dc) control applications [5]. Triggered 96 ksps and 1 Msps waveform records are beyond the scope of this paper.

While these three types of real-time measurements differ substantially in their frequency-domain resolution, they can provide real-time power quality monitoring and situational awareness of the power system. Figure 3(a), Figure 3(b), Figure 3(c), and Figure 3(d) show the SCADA, PMU, and WMU captures for a substation bus load change event. As seen in Figure 3(a), SCADA captures a step change in the three-phase load current magnitudes while the three-phase voltages rapidly decrease. Even though SCADA captures the magnitude changes in voltages and currents, the data may not include a

high enough resolution to obtain the desired insight and cause of the step load change.

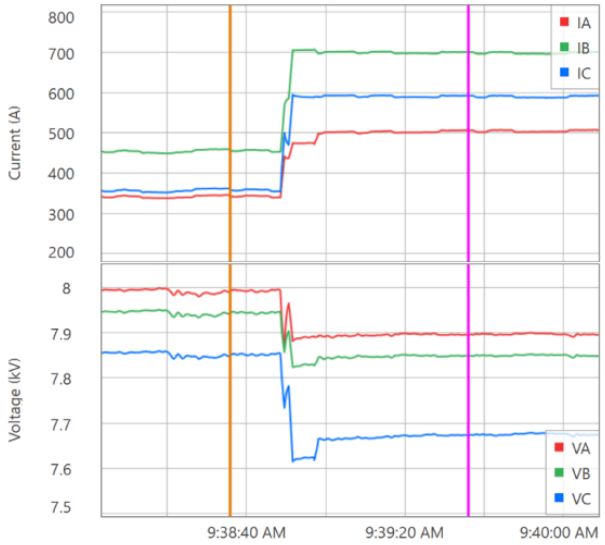

(a) SCADA

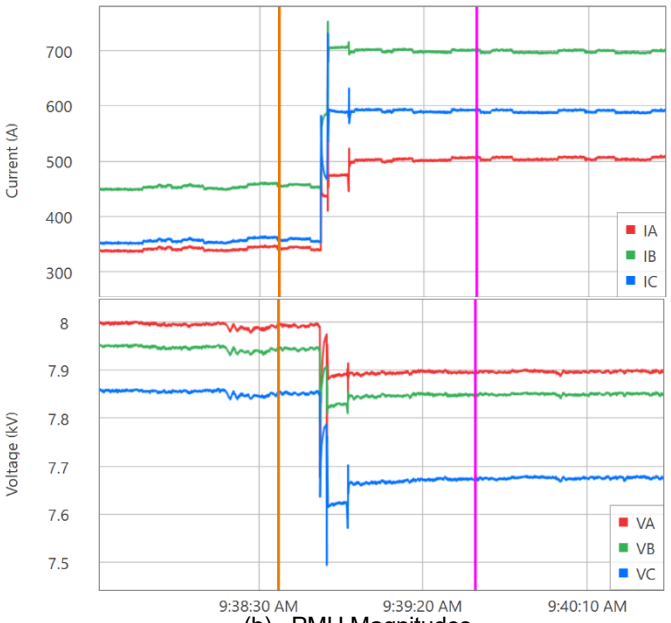

(b) PMU Magnitudes

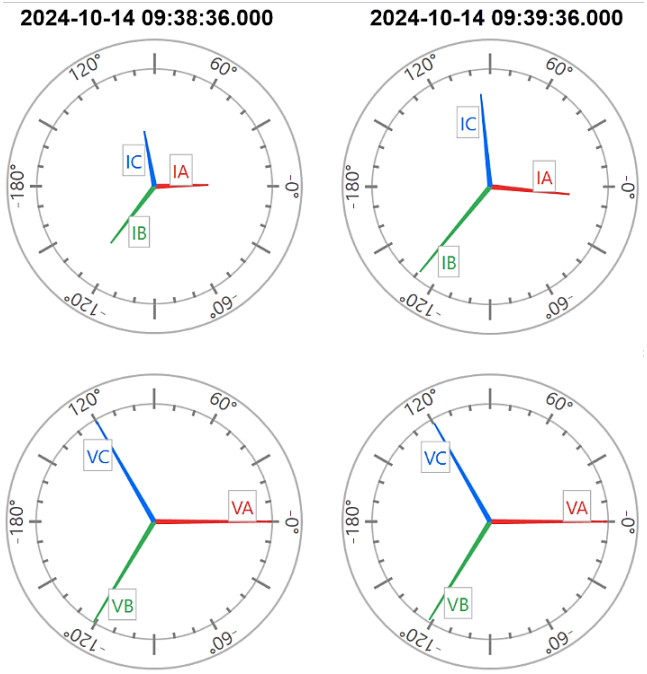

(c) PMU Phasors

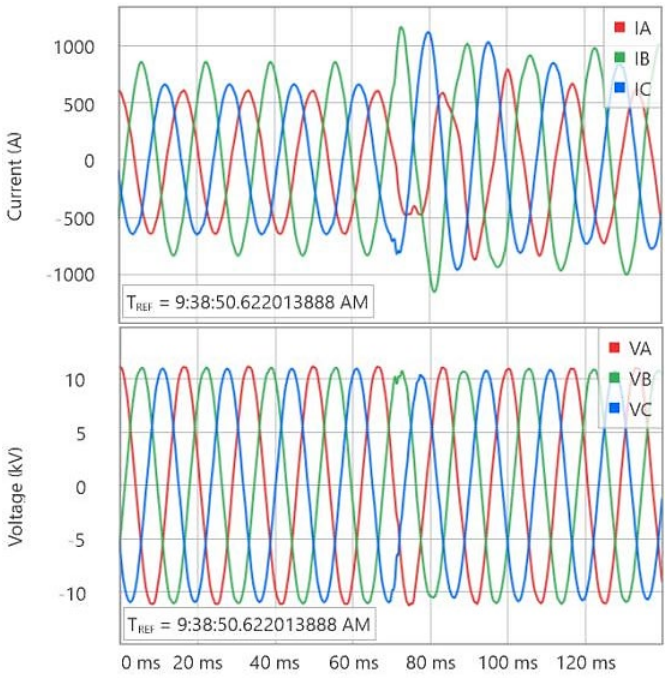

(d) WMUs

Figure 3 Comparison of Signal Data From (a) SCADA, (b) PMU Magnitudes, (c) PMU Phasors, and (d) WMUs

The phasors to the left in Figure 3(c) correspond to the left (orange) time cursor in Figure 3(b) and represent the steady-state three-phase voltages and currents prior to the load change event. Similarly, the phasors to the right in Figure 3(c) represent the steady-state currents and voltages after the load change and correspond to the right (magenta) cursor in Figure 3(b). A comparison of these two sets of phasors identifies that the currents increased following the load change while the voltage magnitudes slightly dropped, as shown in TABLE I.

TABLE I
2024-10-14 PMU MEASUREMENTS[a]

Signal	09:38:36	09:39:36	ΔM[b]	Δ%
VA (kV)	8.00∠0°	7.90∠0°	–0.10	–1.2
VB (kV)	7.95∠–121°	7.85∠–122°	–0.10	–1.2
VC (kV)	7.85∠119°	7.67∠120°	–0.18	–2.3
IA (A)	343∠2°	506∠–5°	163	48
IB (A)	456∠–127°	701∠–129°	244	54
IC (A)	359∠101°	592∠96°	234	65

[a] Shown in Figure 3(c) and discussed in Section IV-E.
[b] Difference in signal magnitude before and after a load change.

In addition to the magnitude changes, PMU measurements also provide the phase-angle (position of waveform in time) relationships between the different signals. The phase-angle difference between the voltage and current signals can be used to determine the system's power factor. Additionally, active power flows from the bus with the higher-voltage phase angle (leading voltage waveform) to the bus with the lower-voltage phase angle (lagging voltage waveform). This way, PMU measurements can be used to monitor power flow across transmission lines and the wider electrical system. This is a key advantage of PMU data over SCADA data. Figure 3(d) shows the same step load change event as captured by a WMU. In addition to the changes in the magnitudes and angles, signals shape of the disturbance in the current and voltage waveform plots are now observable. This way, WMUs offer a way to capture the transient characteristic of a disturbance and a more detailed system response.

High-resolution waveform measurements enable a diverse range of applications, including the analysis of inverter-based resources' impact in protection mechanisms, dynamic response studies, the detection of incipient faults, the localization of partial discharge and arcing, wildfire monitoring, and the estimation and validation of network parameters [8]. The use cases of waveform recordings are well defined in reports [3] and [9] and in technical papers [7] and [13]. Some previously published examples are highlighted in the following paragraphs.

Figure 1 in [11] shows the three-phase instantaneous power in megawatts at both ends of a 345 kV series-compensated transmission line with two visible phenomena: an amplitude-modulated ripple and a high-frequency distortion. Power quality instruments that employ a 1 cycle or 200 ms average power measurement simply average the sampled measurements of these two distortions and represent the signal as a nearly flat line. With a WMU, the terminal current waveforms in Figure 4 in [11] and the voltage waveforms in Figure 6 in [11] clearly show the nonsinusoidal and slightly unbalanced nature of the signals.

Figure 2.1 in [14] shows a time-domain plot of voltage waveforms recorded during the August 2016 Blue Cut Fire after 1,200 MW of photovoltaic generation units either disconnected or switched into momentary cessation mode. This view of the waveforms enables the quick observation and measurement of the four instantaneous phase shifts (or phase jumps), sags, and harmonic distortions in the three-phase voltage waveform signals.

Past research efforts suggest that waveform measurements can enable users to make situational awareness actions proactive, instead of reactive. Due to gradual insulation breakdown, incipient cable faults typically occur before the permanent failure of the cable or cable joint [8] and can be difficult to detect prior to permanent cable failure. It is common for self-clearing faults to last about one-half cycle, Figure 4(b) of [15] shows an example of using the voltage and current waveform signals to observe a half-cycle (8.3 ms), self-clearing incipient cable fault.

III. DERIVING PMU SIGNALS FROM WMU SIGNALS

Synchrophasor data collected by PMUs across an interconnected power network provide a useful overview of system conditions. Additional quantities are calculated from the voltage and/or current phasors, including fundamental active power, apparent power, and power factor; frequency; rate-of-change of frequency (ROCOF); and sequence (symmetrical) components. Conventional PMUs calculate synchrophasors from digitally sampled analog waveforms. With a WMU, the CWR software can calculate synchrophasors from the waveform data. This approach allows operators to retain the benefits of waveform measurement and synchrophasor data while eliminating the need to transmit both data types.

A. Signal Processing

The digital signal processing path for calculating synchrophasors in the CWR software is shown in Figure 4. This processing path is similar to the process in a PMU's firmware. Discrete time and value pairs from the received current and voltage waveform data are converted to phasor values by modulating a Coordinated Universal Time (UTC)-synchronized complex exponential signal. These values are passed through a low-pass (LP) filter with a 3 dB point of 22 Hz. The magnitude and angle output values are then stored in the software historian at the same rate as the nominal frequency and aligned to the top of the second (the beginning of a new UTC second) [10].

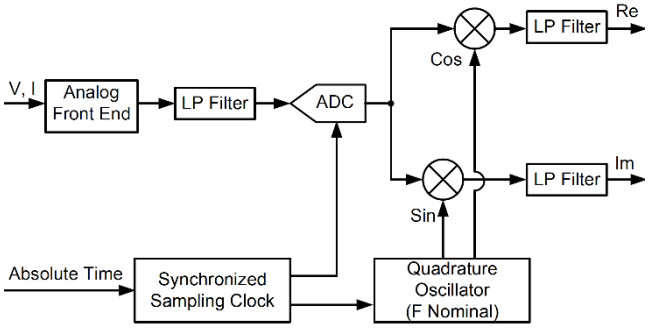

Figure 4 Synchrophasor Calculation [10]

Frequency, ROCOF, power, and sequence components are all derived from the phasor values. All values are available for monitoring and analysis alongside the stored data from synchrophasor streams from conventional PMUs.

B. PMU Signal Content

Waveform measurement signals input to the PMU software can be characterized via their Fourier transform with (1):

$$X(t) = \sum_{n=1-n_{max}}^{n_{max}-1} A_n e^{j\bullet(n\omega_0 t+\phi_n)} \quad (1)$$

where:

$\omega_0 = {}^{2\pi}/_{\tau}$, $n_{max} = \frac{f_s\tau}{2}$.

f_s is the sampling frequency.

τ is the duration of the window of the signal considered in seconds.

Modulating the signal by a nominal frequency complex exponential shifts every frequency by 60 Hz, resulting in two frequency-domain images of the original signal, one centered at 0 Hz and the other at 120 Hz. Therefore, the LP filter, with a cutoff at 22 Hz, leaves the portion of the signal centered at 0 Hz (i.e., the frequency components originally between 38 and 82 Hz) intact and removes the copy at 120 Hz. Fundamental frequency signals remain intact, but harmonics, interharmonics above 82 Hz, and low-frequency content do not.

Different synchrophasor algorithms use LP filters with different cutoffs. However, [10] requires that the 90 Hz signals be attenuated for measurement-class PMUs and 120 Hz signals be attenuated for protection-class PMUs. This means that no PMU measures signal components greater than twice the nominal frequency. Waveform measurements, by contrast, are able to retain the spectrum up to $f_s/2$. For a 14.4 ksps data rate, frequency content up to 7.2 kHz is present in the data.

IV. FIELD EXPERIENCE

The field waveform recordings in this section are obtained from an electric power intensive iron casting industrial plant that utilizes electric induction furnaces in its processes. This plant was selected to perform a field trial in the hope that the CWS&R system could detect transients on one of two main 13.8 kV buses that supply the entire plant. Part A is a comparison of using waveform measurement data versus voltage sag, swell, or interruption (VSSI) recorder-triggered data. Part B explains a transient switching event that occurs between two steady-state load conditions. Part C describes a one-cycle duration transient event that occurs due to the medium-voltage capacitor bank stage closing. Part D shows the application of incremental quantity (IQ) disturbance monitoring in the CWR software application. Part E provides insight into the derived PMU measurements at steady state during a period of bus load variation.

A. Event 1—Comparison of WMU Data With VSSI Detection

VSSI recorders frequently use short-duration, 16 spc triggered recordings. Depending on the trigger configuration, VSSI reports can miss extremely high-frequency voltage transients. After weeks of failed attempts to capture suspected transients in the system using a VSSI recorder, the plant engineer installed a WMU. On September 17, 2024, at 15:05:01 CDT, the plant engineer was able to capture a transient during a load change event. Figure 5 shows the transient event captured by the WMU at 14.4 ksps. Also shown on the plot is what a VSSI recorder would capture after applying anti-aliasing filters and downsampling the WMU measurements to 16 spc. A comparison of the respective one-cycle root-mean-square (rms) magnitudes shows why the VSSI recorder might not trigger on this event. The result of the one-cycle sliding window rms calculation specified in [4] is shown in Figure 6. The rms value of the downsampled waveform is 0.04 per unit (pu) lower than that of the 14.4 ksps waveform—in fact, the 16 spc waveform does not reach 1.05 pu, a common threshold for VSSI detection.

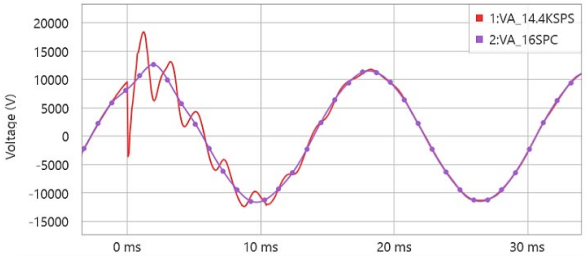

Figure 5 14.4 ksps Vs. 16 spc Waveform

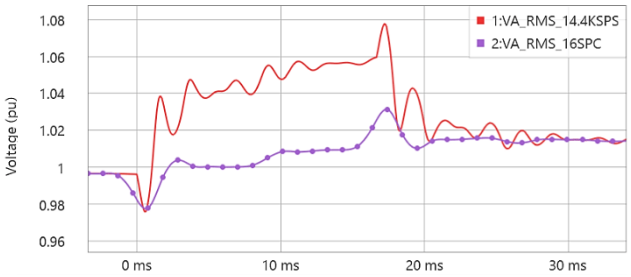

Figure 6 14.4 ksps Vs. 16 spc rms Calculation

B. Event 1—Load Increase With Harmonic Decrease

Figure 7 shows the current waveform signals, and Figure 8 shows the one-cycle rms magnitudes from the load change event captured on September 17, 2024, at 15:05:01 CDT.

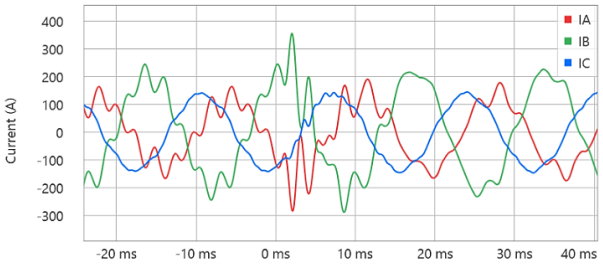

Figure 7 Current Waveform Signals

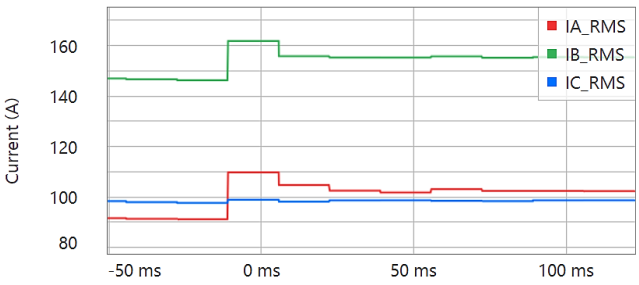

Figure 8 rms Current Magnitudes

In Figure 8, it is clear that Phase B is loaded more than the other two phases, even prior to the load change. The rms current magnitude rises for Phases A and B and remains steady for Phase C.

However, looking at separate harmonics shows a different picture. Following the load change, the seventh-harmonic content drops from approximately 25 A to approximately 7 A in Phases A and B, as seen in Figure 9. In Phase C, the seventh-harmonic content drops from around approximately 4 A to 1 A. This represents a change in the seventh-harmonic content from 29 percent of the fundamental to 7 percent of the fundamental in Phases A and B, which is a drastic improvement. Measuring harmonics is not possible with synchrophasors, which demonstrates the value of WMUs.

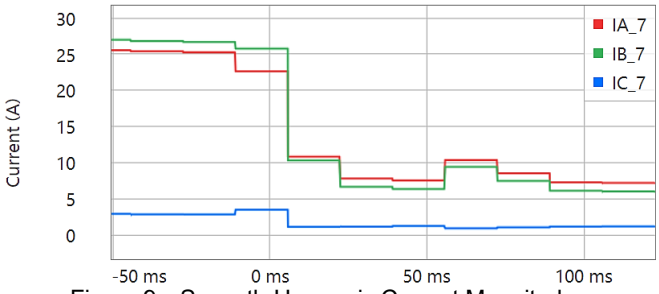

Figure 9 Seventh-Harmonic Current Magnitudes

C. *Event 2—Capacitor Bank Switch-In*

On Monday, September 23, 2024, the system captured a transient between two steady states, as seen in Figure 10 and Figure 11.

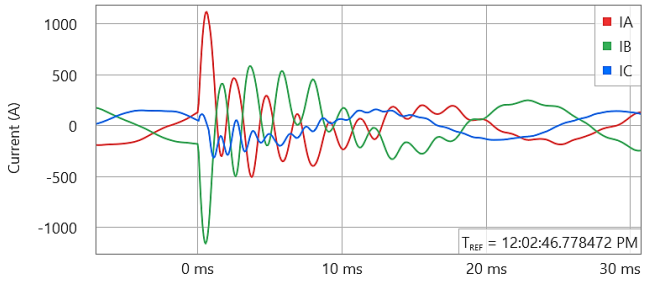

Figure 10 Current Waveforms at the Time of Closing

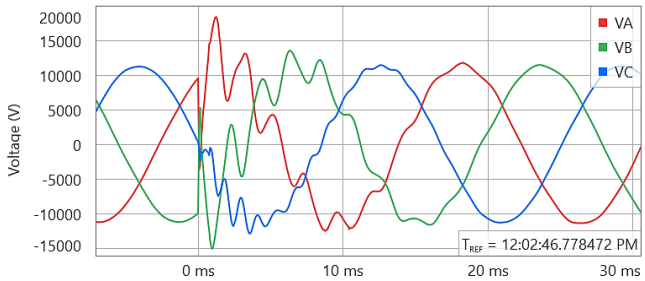

Figure 11 Voltage Waveforms at the Time of Closing

The voltages on all three phases drop past zero, as seen in Figure 12. The instantaneous voltage dropping to zero is a signature of capacitor insertion [16]. These voltages dropping to zero then continuing past to the opposite polarity indicates that the capacitors likely had some residual voltage before the switching event.

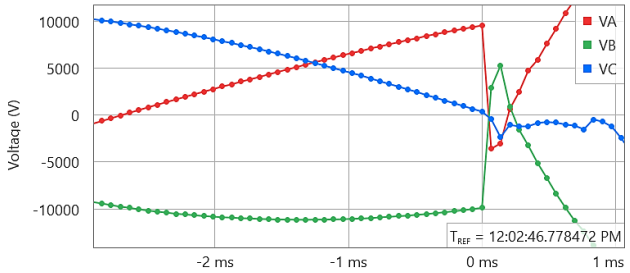

Figure 12 Voltage Transient Overshoots Zero

This event illustrates the usefulness of having both the WMU and the PMU synchrophasor data. These data were used to calculate the capacitance and inductance involved in the transient. The voltage and current phasors were first calculated using a synchrophasor filter, as explained in Section III. Then, after using (2), the adjusted (ϕ_{new}) angles accounted for the fact that the system frequency was not exactly at 60 Hz:

$$\phi_{new}(t) = \phi_{old}(t) - 2\pi\Delta f \bullet t \tag{2}$$

where Δf is the difference between the nominal and the actual frequency.

The adjusted angles were used to calculate the difference between the per-phase reactive power before and after the transient (ΔQ). Per-phase capacitance (C) is calculated according to (3):

$$C = \frac{\Delta Q}{2\pi f V^2} \tag{3}$$

Note that the capacitance and reactive power of Phase C are about one-third that of Phases A and B. All of the preceding analysis could be done with just the synchrophasor measurements. However, with waveform measurements, it is possible to measure the transient itself. The authors obtained the disturbance signal (i.e., the deviation from a fundamental-only sinusoid), shown in Figure 13, by subtracting the synchrophasor estimated signal from the true signal.

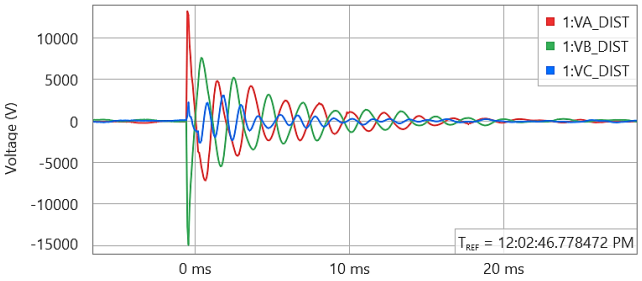

Figure 13 Difference Between Synchrophasor Approximation of Voltage and Actual Voltage

Then, the authors calculated the inductance resonating with the capacitor, the system was assumed to be a resistor, inductor, and capacitor (RLC) circuit, and a curve was fit to the disturbance data using (4), where V_{dist} is the disturbance voltage, V_0 is the fundamental voltage, and ω_d is the resonant angular frequency.

$$V_{dist}(t) = V_0 e^{-\alpha t} \sin(\omega_d t + \phi) \quad (4)$$

From these values, ω_0 is calculated, using (5):

$$\omega_0 = \sqrt{(\omega_d^2 + \alpha^2)} \quad (5)$$

where α is the attenuation constant.

Using (5) and the fit values of α = 240 and ω_d = 2π·480 rad/s, yields ω_0 = 2π·481.52 rad/s. The inductance (L) oscillating with the capacitor on each phase is defined using (6):

$$\omega_0 = \frac{1}{\sqrt{LC}} \quad (6)$$

Substituting the values for ω_0 and capacitance (C) yields the inductances in the millihenry (mH) range. A value was not calculated for Phase C because it was a small transient and did not fit an RLC circuit well. The per-phase capacitances of the capacitor bank agree with the results from (3) calculated in TABLE II. At the time of this event, several stages of the capacitor bank were already out of service due to blown fuses, as shown in Figure 14. This explains the low value of the Phase C capacitance in TABLE II.

Figure 14 Blown Fuses on the Capacitor Bank

TABLE II
CALCULATED ΔQ, C, AND L

Phase	A	B	C
ΔQ (MVAR)	1.87	1.79	0.60
Capacitance (μF)	38.0	36.7	12.5
Inductance (mH)	2.9	3.0	N/A

D. IQs Disturbance Monitoring

In September 2024, the authors needed a way to make disturbances stand out during a visual inspection of an hour or longer of raw waveform signals within the CWR software. The authors used the IQs, also known as differential waveforms [7], of each of the voltage and current signals for better transient detection. IQs are obtained by extracting the superimposed transient event component samples for a power cycle from the previous undisturbed power cycle of samples. Applied to a 60 Hz system, the fixed 14.4 ksps reporting rate equates to 240 samples of waveform measurements in one power system cycle or 240 spc. So, each IQ measurement sample is obtained by simply subtracting the prior measurement sample (k = 1) from the present measurement sample (k = 241), using (7).

$$\mathrm{IQx[k]} = \mathrm{x[k]} - \mathrm{x[k-240]} \quad (7)$$

Figure 15 shows the dashboard view of the three-phase current and three voltage IQ signals, from 19:00:00 CDT to 23:00:00 CDT on Saturday, October 5, 2024. From this view, the authors counted the number of transients and measured the duration between transients. Forty-three transients are observed in the four hours shown in Figure 15, which corresponds to an average of one transient every 5 to 6 minutes.

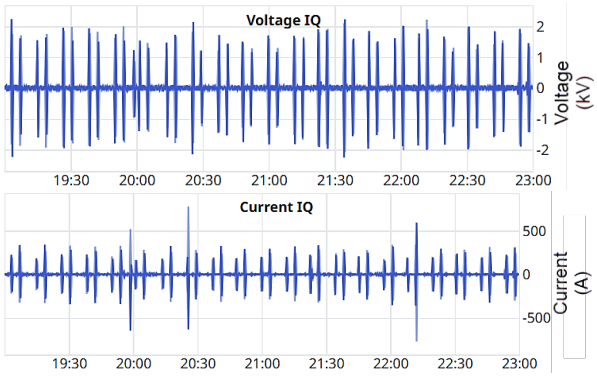

Figure 15 IQ Disturbance Dashboard

Furthermore, this rapid and instant detection method ensured all transient events that occurred on the monitored medium-voltage bus in the plant's distribution system were easily observed. Previous attempts to monitor transients on the same bus using triggered power quality monitoring for 72 hours had failed, likely due to the power quality trigger conditions not being sensitive enough to detect one-cycle switching transients.

Further modal analysis on the IQ signals may better explain the transient disturbance.

E. Derived PMU Measurements

Analysis of the derived one-cycle PMU measurements from October 14, 2024, a day with no observed system disturbances, provides insight into the power demand of the processes used at the study site. An analysis of the sample ranges from 09:37:36 to 09:57:35 CDT on October 14, 2024, is shown in Figure 16.

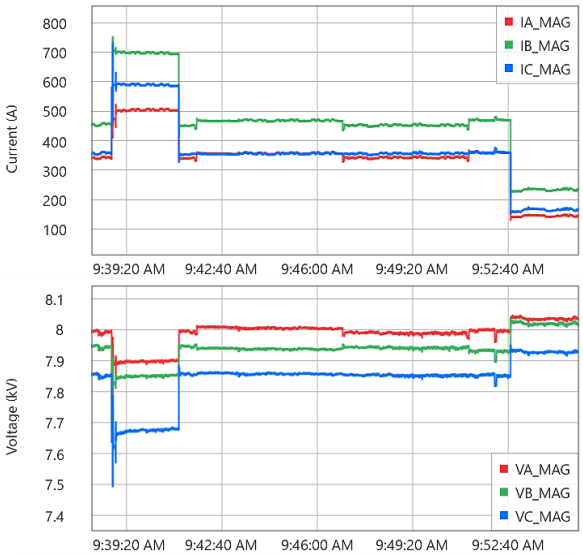

Figure 16 Derived PMU Measurements on 2024-10-14 at 09:37:36

The authors applied a 600-sample (10 s) boxcar filter, i.e., a simple moving average of the previous N samples, to the derived PMU measurements to smooth them further, creating 10 s window PMU measurements.

The authors took five samples from specific sections of the boxcar-filtered signals to use in the analysis:

1. 09:38:36.000
2. 09:39:35.000
3. 09:42:25.000
4. 09:52:31.000
5. 09:53:53.000

Each of these five samples corresponds to a different system state, as noted in Figure 17. The difference between the current demands at each sample is evident. The highest value of 700 A is on Phase B at 09:39:35, and the lowest value of 235 A is on Phase B at 09:53:53. With further investigation, it may be possible to identify the specific processes that were starting and stopping at the plant at these times. This would allow plant engineers to learn the characteristics of various loads. Changes in the load characteristics could provide early warnings of failing equipment.

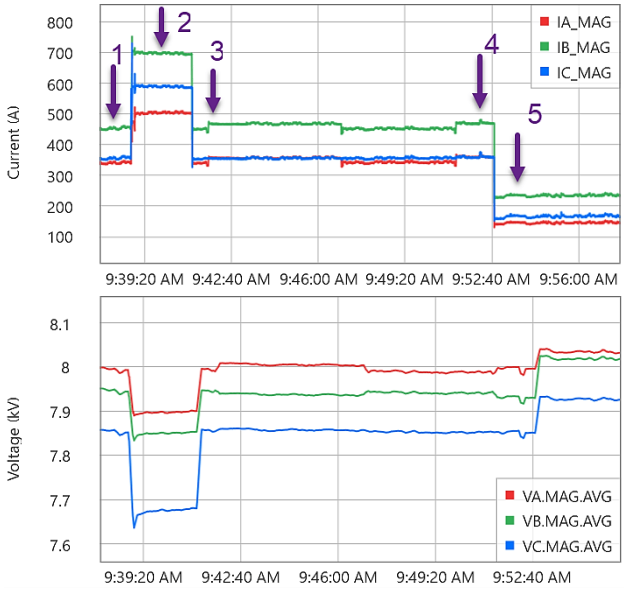

Figure 17 Boxcar PMU Measurements

Information from these synchrophasor plots could be used to improve plant power quality and utilization. There is a significant unbalance in the phase loading; Phase B is the most heavily loaded, and Phase A is the most lightly loaded. There is also noticeable voltage unbalance, which could be caused by the unbalanced phase loading. Plant engineers can estimate the amount of unbalance in the three-phase voltages by calculating the negative-sequence voltage. At 09:39:35, the Phase C voltage is below 7.7 kV, while the other two phases are above 7.8 kV. The negative-sequence voltage at this time is approximately 137 V, which is about 1.8 percent unbalance. At 09:38:36 and 09:42:25, there was only 1.1 percent unbalance, so this is noticeably different from the other sampled times. With more information from other PMUs and a longer study, it could be possible to identify the specific processes and equipment that cause this uneven phase loading. Using this information, a plant manager could rebalance single-phase loads to better balance the plant distribution circuits.

V. BANDWIDTH AND STORAGE CONSIDERATIONS

A. Overview

CWS has higher bandwidth and storage requirements than other types of real-time power system data. The requirements generally scale linearly with the resolution of the data and the number of signals provided. Modern networks are well equipped for the network traffic of CWR systems, which typically ranges from hundreds to thousands of kilobits per second and is comparable to audio or video streaming. The disk space requirements of days or weeks of continuous waveform data may exceed the capacity of typical industrial-grade solid-state drives. Storing this quantity of data on a traditional power quality meter with 1 or 2 gigabytes of onboard storage is out of the question, which is why it is essential to have continuous connectivity to the streaming receiver. Server or secure cloud storage solutions can assist with storing longer durations of data, such as weeks or months. Even so, storing years of data, as is typical for oscillography and load profile data, may not be feasible.

The required network bandwidth for CWS depends on four factors: protocol overhead, the number of analog values, bits per analog, and the streamed sample rate. To reduce the overhead, creators of WMUs choose streaming protocols that have the lowest overhead necessary for their needs. The high sample rate of continuous waveform data is its primary benefit over other types of real-time power system data, and it is also the primary reason for its high-bandwidth requirement. Bandwidth is usually expressed in bits per second (bps).

When continuous waveform data are stored, there is an additional factor of duration of data stored and an added concern of speed of data retrieval. Data should be stored for the duration needed and at the required resolution. For example, continuous waveform data in their raw form may have limited use for long-term load trending, whereas aggregated 15-minute current rms data would be much better suited for this task. If a consumer of continuous waveform data desired to compare load trends from one year to the next, several years of 15-minute rms data would both be more useful and take up 1/12,960,000th the disk storage. Conversely, a transmission operator may want to see a low-impedance fault signature at the full, raw resolution of thousands of samples per second, but may not need more than a few recent weeks of archived data. A single timespan of continuous waveform data can be stored at multiple resolutions simultaneously, which allows users to view data at the most appropriate resolution for their needs. Additionally, this provides users with more granular control over the amount of data stored.

B. Network Bandwidth Requirements

The required network bandwidth for CWS depends on four factors: protocol overhead (OH), number of different analog values (NOA) provided, bits per analog (bits/A), and the streamed sample rate (f_s). The required bandwidth (BW) in bps is given by (8):

$$\mathrm{BW} = \left(\mathrm{OH} + (\mathrm{NOA} \bullet \mathrm{bits/A})\right) \bullet f_S \qquad (8)$$

The WMU used to capture the field data in Section IV streams 17 different analog signals at 14.4 ksps. These 17 analog signals are listed in TABLE III. Each data point is a 32-bit IEEE 754 [17] floating-point value.

By substituting values into (8), the required network BW for this WMU equals (9):

$$\begin{aligned} \text{BW} &= \big(224 + (17 \bullet 32)\big) \bullet 14{,}400 \text{ bps} \\ &= 11{,}059 \text{ kilobits/second} \end{aligned} \quad (9)$$

The 17 instantaneous analog CWS signals produced by the WMU are listed in order by tag with the unit and description in TABLE III:

TABLE III
INSTANTANEOUS ANALOG CWS SIGNALS

Tag	Units	Description
VA	Volts (V)	Phase A, Voltage
VB	V	Phase B, Voltage
VC	V	Phase C, Voltage
VN	V	Phase N, Voltage
IA	Amperes (A)	Phase A, Current
IB	A	Phase B, Current
IC	A	Phase C, Current
IN	A	Phase N, Current
IA_UCS[a]	A	Phase A, Fault Current
IB_UCS[a]	A	Phase B, Fault Current
IC_UCS[a]	A	Phase C, Fault Current
IN_UCS[a]	A	Phase N, Fault Current
AI_1	A	Channel 1, Analog In
AI_2	A	Channel 2, Analog In
AI_3	A	Channel 3, Analog In
AI-4	A	Channel 4, Analog In
V_AUX	V	Auxiliary, Voltage

[a] The universal current sensor (UCS) signal measures the full-spectrum alternating current (ac) and dc signals in a higher fault current range than the load current channels (IA, IB, IC, and IN), with less accuracy.

C. Storage Requirements

Stream storage size (SSS), which is the storage requirement for one stream of recorded data, has a similar equation to BW in (8) but with the additional multiplier of duration of data (DD) stored, as shown in (10). Equation (10) gives storage in bytes.

$$\text{SSS} = \text{NOA} \bullet (\text{OH} + (\text{f}_\text{S} \bullet \text{DD} \bullet \text{Bytes/A})) \quad (10)$$

Using (10), the required per-day SSS equals (11):

$$\begin{aligned} \text{SSS} &= 17 \bullet \big(50{,}000 + (14{,}400 \bullet 86{,}400 \bullet 4)\big) \\ &= 84.6 \text{ gigabytes/day} \end{aligned} \quad (11)$$

There is additional usage of 30 GB/day total for the IQ signals, which corresponds to the three phase-to-neutral voltages and the three-phase currents.

VI. CONCLUSION

Limitations to the capabilities of continuous waveform monitoring, such as high storage and bandwidth requirements, lack of availability of WMUs, lack of receivers, and challenges in analyzing large quantities of data, are beginning to be overcome by the following improvements: commercially available data storage and streaming solutions, standardization of WMUs, software applications for receiving and recording continuous waveform signals, and analytical software tools with digital signal processing capabilities. The benefits of CWR versus event-triggered waveform signals include more sensitive voltage dip and swell detection, one-cycle duration transient event detection, and IQ disturbance monitoring.

The authors foresee further value and usefulness with the application of waveform recording systems as the application software is further improved to programmatically time-stamp, produce dashboard notifications, and provide insight within the notification that identifies not only the power quality condition of the notification but also the likely source location or direction of disturbance or incipient failure and the power system equipment component involved.

While not considered in this paper, situational insight of an entire industrial plant could be accomplished using the time-synchronized signals from numerous WMUs located throughout the entire power system. The WMUs could be at different voltage levels for more comprehensive waveform data and monitoring of all sources and loads.

VII. ACKNOWLEDGEMENTS

The authors thank Palmer Tetley of American Castings in Pryor, OK, for his collaboration, field application, field data collection, and assistance with the field experience portion of this paper.

The authors also thank Dr. Ellery Blood of Schweitzer Engineering Laboratories, Inc., for his assistance with the analysis and review of this paper.

VIII. REFERENCES

[1] F. Choudhury, M. Yalla, and G. Rinaldi, “Analysis of Power Quality Monitoring Methods in Industrial Distribution Systems,” proceedings of the 71st Annual Petroleum and Chemical Industry Technical Conference, Orlando, FL, September 2024.

[2] I. C. Evans, “The Perils of Offshore Power Quality,” September 2014. Online at OEDigital.com.

[3] J. Follum, L. Miller, P. Etingov, H. Kirkham, A. Riepnieks, X. Fan, and E. Ellwein, “Phasors or Waveforms: Considerations for Choosing Measurements to Match Your Application,” Pacific Northwest National Laboratory, Technical Report PNNL-31215, April 2021.

[4] IEC 61000-4-30:2015, *Electromagnetic Compatibility (EMC)* – Part 4-30: Testing and Measurement Techniques - Power Quality Measurement Methods.

[5] IEC 61869-9:2019, *Instrument Transformers* – Part 9: Digital Interface for Instrument Transformers, 2019.

[6] E. O. Schweitzer, III, D. E. Whitehead, G. Zweigle, V. Skendzic, and S. V. Achanta, “Millisecond, Microsecond, Nanosecond: What Can We Do With More Precise Time?” proceedings of the 42nd Annual Western Protective Relay Conference, Spokane, WA, October 2015.

[7] H. Mohsenian-Rad and W. Xu, “Synchro-Waveforms: A Window to the Future of Power Systems Data Analytics,” *IEEE Power and Energy Magazine*, vol 21, no. 5, pp. 68–77, September 2023.

[8] IEEE PES Task Force on Big Data Analytics for Synchro-Waveform Measurements, “Synchro-Waveform Measurements and Data Analytics in Power Systems,” IEEE PES, Technical Report PES-TR127, December 2024.

[9] A. Silverstein and J. Follum, “High-Resolution, Time-Synchronized Grid Monitoring Devices,” North American Synchrophasor Initiative, Technical Report PNNL-29770/NASPI-2020-TR-004, March 2020.

[10] IEEE/IEC 60255-118-1-2018, *International Standard – Measuring Relays and Protection Equipment* - Part 118-1: Synchrophasor for Power Systems – Measurements.

[11] M. J. Lewis and R. D. Kirby, “Energy and Power Measurements on a Nonsinusoidal 345 kV System Using Three-Phase Megahertz Time-Series Data,” proceedings of the Annual Georgia Tech Fault and Disturbance Analysis Conference, Atlanta, GA, May 2023.

[12] M. Lewis, F. Elhaj, and R. Kirby, “UHS Relay Testing for Optimal Protection of a Long 345 kV Line With Series Compensation,” proceedings of the 48th Annual Western Protective Relay Conference, Spokane, WA, October 2021.

[13] A. F. Bastos, S. Santoso, W. Freitas, and W. Xu, “SynchroWaveform Measurement Units and Applications,” proceedings of the IEEE Power and Energy Society General Meeting (PESGM), Atlanta, GA, July 2019.

[14] North American Electric Reliability Corporation, “1200 MW Fault Induced Solar Photovoltaic Resource Interruption Disturbance Report,” June 2017. Online at https://www.nerc.com/pa/rrm/ea/Documents/1200_MW_Fault_Induced_Solar_Photovoltaic_Resource_Interruption_Final.pdf.

[15] Transmission & Distribution Committee, Power Quality Subcommittee, Working Group on Power Quality Data Analytics, “Electric Signatures of Power Equipment Failures,” IEEE PES, Technical Report PES-TR73, December 2019.

[16] S. Santoso, *Fundamentals of Electric Power Quality*, Scotts Valley, CA: CreateSpace Independent Publishing Platform. December 2010.

[17] IEEE 754-2019, *IEEE Standard for Floating-Point Arithmetic*.

IX. VITAE

Richard Kirby, PE (S ’90, M ’96, SM ’06), is a senior engineer at Schweitzer Engineering Laboratories, Inc. (SEL), in Houston, Texas. His focus is waveform measurement, power quality metering, transient recording, and disturbance detection. He is a registered Professional Engineer in Arkansas, Louisiana, Michigan, Oklahoma, and Texas. He has 32 years of diverse electric power engineering experience. He received a BS in engineering from Oral Roberts University in Tulsa, Oklahoma, in 1992, and in 1995, he earned his Master of Engineering in electric power from Rensselaer Polytechnic Institute in Troy, New York. Richard has coauthored eight technical papers.

Ganga Ramesh received her BTech in electrical and electronics engineering from Amrita University in Coimbatore, India, in 2018 and her MSc in electrical engineering from Arizona State University in Tempe, Arizona, in 2020. She currently works for Schweitzer Engineering Laboratories, Inc. (SEL), as a protection application engineer in Houston, Texas.

Phil Stoaks is a lead engineer at Schweitzer Engineering Laboratories, Inc. (SEL), in Boise, Idaho, where he is a member of the R&D Meters Software team. He works to develop software solutions for applying data collected by meters and power monitors. He received a BS in biology from Eastern Oregon University in La Grande, Oregon, in 2013.

Drew Cannon received a BS degree in physics and an MS degree in electrical engineering from Washington State University in 2019 and 2021, respectively. Since 2022, he has worked as a power engineer at Schweitzer Engineering Laboratories, Inc. (SEL). His interests include theory and applications of measurement algorithms.

Previously presented at the 72nd Annual Petroleum and Chemical Industry Technical Conference, Dallas, Texas, September 2025.

20250403 • TP7193